

Modulational instability in a layered Kerr medium: Theory and Experiment

Martin Centurion<sup>1,2</sup>, Mason A. Porter<sup>2,3</sup>, Ye Pu<sup>1</sup>, P. G. Kevrekidis<sup>4</sup>, D. J. Frantzeskakis<sup>5</sup>, and Demetri Psaltis<sup>1</sup>

<sup>1</sup>Department of Electrical Engineering, <sup>2</sup>Center for the Physics of Information,

<sup>3</sup> Department of Physics, California Institute of Technology, Pasadena, CA 91125, USA

<sup>4</sup>Department of Mathematics and Statistics, University of Massachusetts, Amherst MA 01003-4515, USA  
<sup>5</sup>Department of Physics, University of Athens, Panepistimiopolis, Zografos, Athens 15784, Greece

We present the first experimental investigation of modulational instability in a layered Kerr medium. The particularly interesting and appealing feature of our configuration, consisting of alternating glass-air layers, is the piecewise-constant nature of the material properties, which allows a theoretical linear stability analysis leading to a Kronig-Penney equation whose forbidden bands correspond to the modulationally unstable regimes. We find very good *quantitative* agreement between theoretical, numerical, and experimental diagnostics of the modulational instability.

PACS numbers: 05.45.Yv, 42.65.Sf, 42.65.Tg, 42.65.-k

*Introduction.* The modulational instability (MI) is a destabilization mechanism for plane waves. It leads to delocalization in momentum space and, in turn, to localization in position space and the formation of solitary-wave structures. It arises in numerous physical contexts, including fluid dynamics [1], nonlinear optics [2, 3], plasma physics [4], and atomic physics [in studies of Bose-Einstein condensates (BECs) [5]].

The MI was originally analyzed in uniform media, mainly in the framework of the nonlinear Schrödinger equation, where a focusing nonlinearity leads to MI for sufficiently large plane-wave amplitudes (for a given wavenumber) or sufficiently small wavenumbers (for a given amplitude) [3]. More recently, several very interesting experimentally relevant settings with (temporally and/or spatially) *nonuniform* media have emerged. Research in this direction includes the experimental observation of bright matter-wave soliton trains in BECs [6], induced by the temporal change of the interatomic interaction from repulsive to attractive through Feshbach resonances. This effective change of the nonlinearity from defocusing to focusing leads to the onset of MI and the formation of the soliton trains [7]. Soliton trains can also be induced in optical settings, as has been discussed, e.g., for birefringent dispersive media [8]. Even closer to this Letter's theme of periodic nonuniformities is the increasingly vast research in photonic crystals [9] and the recent experimental observations of the MI in spatially periodic optical media (waveguide arrays) [10] and BECs in spatially periodic optical lattices [11]. A key feature in such settings is that MI can even occur for defocusing nonlinearities for certain wavenumber bands [12].

In contrast to the aforementioned results, in which the periodicity is in the transverse dimensions, we offer in this Letter the first experimental realization of MI in a setting that is periodic in the *evolution variable* (which here is the propagation distance). Such settings were initially proposed in the context of optics through dispersion management (see, e.g., [13] for reviews) and have since also been studied for nonlinearity management [14, 15]. They

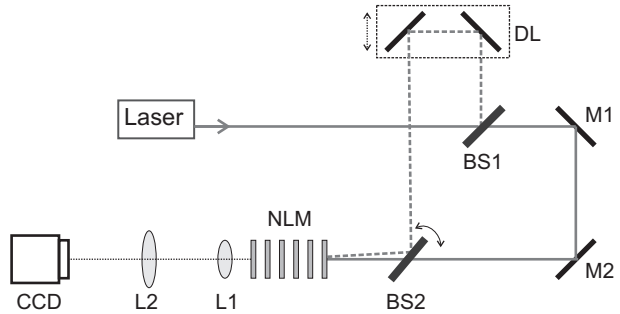


FIG. 1: Experimental setup. BS1 and BS2 are beam splitters, DL is a variable delay line, M1 and M2 are mirrors, NLM is the layered nonlinear medium, and L1 and L2 are lenses.

have also been studied in BECs through so-called Feshbach Resonance Management [16]. In addition to our experiments, we perform direct numerical simulations and a linear stability analysis [16, 17, 18], which leads to a Hill equation [19], whose coefficients are periodic in the evolution variable. The permissible spectral bands of this equation correspond to modulationally stable wavenumbers, and the forbidden bands indicate MI.

Our setup is periodic in the evolution variable; it consists of an optical medium with periodically alternating glass and air layers. The piecewise constant nature of the material coefficients leads to a linear stability condition (for plane waves) along the lines of the Kronig-Penney model of solid state physics [20]. This allows us to compute the MI bands analytically and to compare our experimental findings not only with numerical simulations but also with theoretical calculations.

The rest of this paper is organized as follows. We first present our experimental setup. We then analyze the system theoretically and compare the results of experiments and theory to those of numerical simulations. Finally we summarize our findings and present our conclusions.

*Experimental Setup.* In our experiments (see the schematic diagram in Fig. 1), an amplified Titanium:Sapphire laser is used to generate 150-femtosecond

pulses with an energy of 2 mJ at a wavelength of  $\lambda = 800$  nm. The beam profile is approximately Gaussian with a full-width at half-maximum of 1.5 mm. The laser pulses are split into a pump and a reference using a beam splitter (BS1), with most of the energy in the pump pulse. After synchronization with a variable delay line (DL), the two pulses are recombined at a second beam splitter (BS2) and sent to the periodic nonlinear medium (NLM). The reference introduces a sinusoidal modulation in the intensity (that is, an interference pattern), with the period determined by the relative angle between the two beams. The angle of the reference is carefully tuned by rotating BS2 so that the two beams overlap while propagating through the NLM at adjustable angles. The NLM consists of six 1 mm thick quartz slides separated by air gaps. The glass slides have an anti-reflection coating to minimize the loss. (The transmission for each slide is 98%.) In our experiments, we used structures with air gaps of 2.1 mm and 3.1 mm. The intensity pattern after the NLM (at the output face of the last quartz slide) is imaged on a CCD camera (Pulnix TM-7EX) using two lenses (L1 and L2) in a 4-F configuration, with a magnification of  $M = 8$ . The CCD camera captures the central region (0.6 mm  $\times$  0.8 mm) of the beam.

The intensity pattern at the output of the NLM is recorded both for a high pump intensity of  $I_{P1} = 1.3 \times 10^{11}$  W/cm<sup>2</sup> and a low pump intensity of  $I_{P2} = 9 \times 10^8$  W/cm<sup>2</sup>. In both cases, the intensity of the reference beam is 1% of that of the pump. We measure the effect of the nonlinearity by comparing the output for high versus low intensity. In the latter case, the propagation is essentially linear. If the spatial frequency of the modulation is inside the instability window, the amplitude of the reference wave increases at the expense of the pump.

*Theoretical Setup.* Our theoretical model for the beam propagation incorporates the dominant dispersive and Kerr effects in a nonlinear Schrödinger equation

$$\begin{aligned} i \frac{\partial u}{\partial \zeta} &= -\frac{1}{2} \nabla_{\perp}^2 u - |u|^2 u, \quad 0 < \zeta < \tilde{l} \text{ (glass)}, \\ i \frac{\partial u}{\partial \zeta} &= -\frac{1}{2} \frac{\eta_0^{(1)}}{\eta_0^{(2)}} \nabla_{\perp}^2 u - \frac{\eta_2^{(2)}}{\eta_2^{(1)}} |u|^2 u, \quad \tilde{l} < \zeta < \tilde{L} \text{ (air)}, \end{aligned} \quad (1)$$

where space is rescaled by the wavenumber,  $(\xi, \eta, \zeta) = k^{(1)} \times (x, y, z)$ , and the electric field envelope is rescaled using  $u = (n_2^{(1)} / n_0^{(1)})^{1/2} E$ . The superscript  $(j)$  denotes the medium, with  $j = 1$  for glass and  $j = 2$  for air. The Kerr coefficients of glass and air are  $n_2^{(1)} = 3.2 \times 10^{-16}$  cm<sup>2</sup>/W and  $n_2^{(2)} = 3.2 \times 10^{-19}$  cm<sup>2</sup>/W, respectively. Additionally,  $n_0^{(1)} = 1.5$  and  $n_0^{(2)} = 1$ . The above setting (incorporating the transmission losses at each slide) can be written compactly as

$$i \frac{\partial u}{\partial \zeta} = -\frac{1}{2} D(\zeta) \nabla^2 u - N(\zeta) |u|^2 u - i \gamma(\zeta) u, \quad (2)$$

where  $D(\zeta)$  and  $N(\zeta)$  are piecewise constant functions in consonance with Eq. (1) and  $\gamma(\zeta)$  is the loss rate. Equation (2) possesses plane wave solutions,

$$u_0 = A_0 e^{-\int^{\zeta} \gamma(\zeta') d\zeta'} e^{i A_0^2 \int^{\zeta} N(\zeta') \left( e^{-2 \int^{\zeta'} \gamma(\zeta) d\zeta} \right) d\zeta'}, \quad (3)$$

where  $A_0$  is the initial amplitude. We perform a stability analysis by inserting a Fourier mode decomposition,  $u = u_0(\zeta) [1 + w(\zeta) \cos(k_{\xi} \xi) \cos(k_{\eta} \eta)]$  (where  $w = F + iB$  is a small perturbation), into Eq. (2). Algebraic manipulations then lead to the dynamical equation for  $F$

$$\frac{d^2 F}{d \zeta^2} = \frac{1}{D} \frac{d D}{d \zeta} \frac{d F}{d \zeta} + \left[ -\frac{1}{4} \bar{k}^4 D^2 + N \bar{k}^2 D |u_0|^2 \right] F, \quad (4)$$

where  $\bar{k}^2 = k_{\xi}^2 + k_{\eta}^2$ . While one can analyze Eq. (4) directly, the weak variation of  $D(\zeta)$  can be exploited by substituting  $D(\zeta)$  with its average. [We have checked that this has hardly any effect on the results from Eq. (4)]. Under this additional simplification, Eq. (4) is a Hill equation which, for the piecewise-constant nonlinearity coefficient under consideration, becomes the well-known Kronig-Penney model [20]. This can be solved analytically in both glass and air (with two integration constants for each type of region). We then match the solutions at the glass-air boundaries and obtain matching conditions at  $\zeta = \tilde{l}$  and  $\zeta = \tilde{L}$ . In so doing, we employ Bloch's theorem (and the continuity of  $F$  and  $\frac{dF}{d\zeta}$ ), according to which  $F(\zeta) = e^{-i\omega\zeta} H(\zeta)$ , where  $H$  is a periodic function of period  $\tilde{L}$  [20]. This yields a homogeneous  $4 \times 4$  matrix equation, whose solution gives the following equation for  $\omega$ :

$$\begin{aligned} \cos(\omega \tilde{L}) &= -\frac{s_1^2 + s_2^2}{2s_1 s_2} \sin(s_1 \tilde{l}) \sin[s_2(\tilde{L} - \tilde{l})] \\ &\quad + \cos(s_1 \tilde{l}) \cos[s_2(\tilde{L} - \tilde{l})] \equiv G(\bar{k}), \end{aligned} \quad (5)$$

where  $s_1^2 = \bar{k}^2 D^{(1)} (\bar{k}^2 D^{(1)} / 4 - N^{(1)} |u_0|^2)$  and  $s_2^2 = \bar{k}^2 D^{(2)} (\bar{k}^2 D^{(2)} / 4 - N^{(2)} |u_0|^2)$ . Therefore,  $|G(\bar{k})| \leq 1$  implies stability and  $|G(\bar{k})| > 1$  leads to MI.

*Results.* Before discussing our results, it is necessary to point out two additional assumptions. First, we assume in our numerical simulations that the dynamics is effectively one-dimensional (1D) along the direction of the modulation (i.e., we use  $k_{\eta} = 0$  and vary  $k_{\xi}$ ). Accordingly, we convert the 2D interference patterns recorded on the CCD to 1D ones by integrating along the direction orthogonal to the modulation. Second, we assume that the modulational dynamics of the (weakly decaying) central part of the Gaussian beam of the experiment is similar to that of a plane wave with the same intensity. We tested both assumptions and confirmed them a priori through the dynamical evolution of our experimental and numerical results and a posteriori through their quantitative comparison.

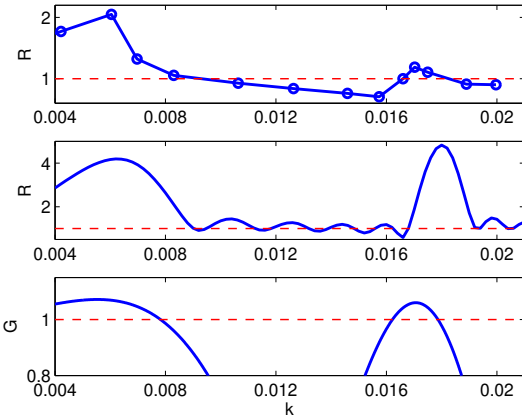


FIG. 2: (Color online) Comparison of experimental (top), numerical (middle), and analytical (bottom) results for the 1 mm glass–2.1 mm air configuration as a function of the dimensionless wavenumber  $k$ . For the diagnostics  $R$  and  $|G|$  (defined in the text), values larger than 1 correspond to MI.

The input field is given by  $u = A_0 + \epsilon_0 \exp(i k_\xi \xi)$ , where  $A_0$  and  $\epsilon_0$  are the amplitudes of the pump and reference beam, respectively, and  $|\epsilon_0|^2 \ll |A_0|^2$ . For linear propagation (low intensity,  $I_{P2}$ ), the intensity pattern at the output of the NLM is approximately the same as that at the input. That is, it is about  $|A_0|^2 + |\epsilon_0|^2 + 2A_0\epsilon_0 \cos(k_\xi \xi)$ . For the nonlinear case (high intensity,  $I_{P1}$ ), higher harmonics are generated and the intensity is about  $|A_1|^2 + 2A_1\epsilon_1 \cos(k_\xi \xi) + 2A_1\epsilon_2 \cos(2k_\xi \xi) + \dots$ , where  $A_1$  and  $\epsilon_n$  ( $n = 1, 2, \dots$ ) are, respectively, the amplitudes of the pump beam and the  $n$ th harmonic at the output of the NLM. The Fourier transform (FT) of this latter intensity is  $|A_1|^2 \delta(f_\xi) + A_1\epsilon_1 \delta(f_\xi - k_\xi/2\pi) + A_1\epsilon_1 \delta(f_\xi + k_\xi/2\pi) + A_1\epsilon_2 \delta(f_\xi - k_\xi/\pi) + A_1\epsilon_2 \delta(f_\xi + k_\xi/\pi) + \dots$ . The ratio of the first and zeroth order peaks in the FT is approximately equal to the ratio of the amplitudes of the reference and pump waves:  $r_1 = \epsilon_1/A_1$  and  $r_2 = \epsilon_0/A_0$ . (For the experimental value of  $\epsilon_0 = A_0/10$ , the error introduced by this approximation is roughly 1%.) The value of  $r_1$  increases with propagation distance as the amplitude of the reference increases. In the linear case,  $r_2$  is constant. We use the ratio  $R = r_1/r_2$  as a diagnostic measure for both our experimental and numerical results (so that  $R > 1$  indicates growth of the perturbation). This measurement is equivalent to the ratio  $r_1(\zeta = \bar{\zeta})/r_1(\zeta = 0)$  (where  $\bar{\zeta}$  is the scaled NLM length), but is more robust experimentally. In the numerical simulations, the peaks in the FT are sharp, whereas they are broader in the experiments. Therefore, when computing  $R$  from the experimental data, we used the area under the peaks instead of the peak value.

Figure 2 shows the ratio  $R(k)$  (where  $k = k_\xi \eta_0^{(1)}$  is the sine of the angle between the pump and reference beams) for the structure with 2.1 mm air spacings. There are two

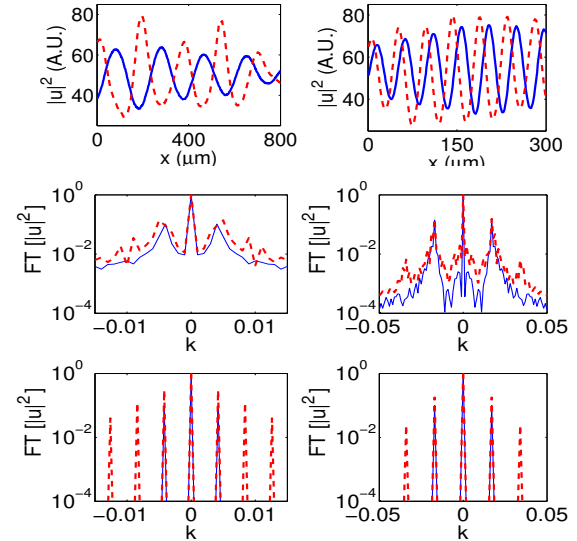


FIG. 3: (Color online) Experimental normalized 1D intensity patterns (top) and Fourier spectra (middle), and numerical Fourier spectra (bottom) at the end of propagation ( $z = 16.5$  mm) of the layered structure with 6 glass slides of 1 mm, each pair of which sandwiches 2.1 mm of air. The left panels show the case of  $k = 0.0042$  (first instability band) and the right panels show the case of  $k = 0.017$  (second band). The dashed curves are for high ( $I_{P1}$ ) intensity and the solid ones are for low ( $I_{P2}$ ) intensity.

instability bands (quantified experimentally by  $R > 1$ ) within the measurement range. The appearance of the second band is a unique feature of the layered medium that originates from the periodicity of the structure in the evolution variable. The maximum growth of the perturbation within the first and second bands appears at  $k = 6.0 \times 10^{-3}$  and  $k = 1.70 \times 10^{-2}$ , respectively. The position of the instability bands is in very good agreement with both numerical and theoretical ( $|G| > 1$ ) predictions. However, the simulation typically shows a stronger instability than the measurement. This results from the 3D nature of the experiment that is not captured in the simulation. In the experiment, the spatial and temporal overlap of the two beams decreases with increasing  $k$ , which leads to weakening of the higher-order peaks. Additionally, the aggregate strength of the nonlinearity in the experiment is reduced due to temporal dispersion. Despite this difference, we stress that the simulations successfully achieve our primary goal of quantitatively capturing the location of the instability windows.

The top panels of Fig. 3 show the normalized 1D intensity pattern at the output of the NLM for  $I_{P1}$  (dashed curve) and  $I_{P2}$  (solid curve). The left panels are for  $k = 4.2 \times 10^{-3}$  (which lies within the first instability band), and the right ones are for  $k = 1.70 \times 10^{-2}$  (in the second band). The amplitude of the modulation increases for the high intensity cases due to MI. We have also ob-

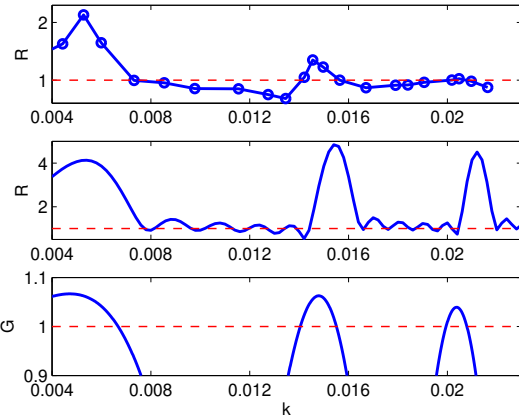


FIG. 4: (Color online) Same as Fig. 2 but for the 1 mm glass-3.1mm air configuration. Here there is a third MI band.

served in the FT of the intensity patterns (middle panels of Fig. 3) the appearance of higher spatial harmonics of the initial modulation, one of the key manifestations of MI, in the instability regions. Such harmonics correspond to the narrowing of the peaks in the spatial interference pattern. The first-order peaks (the ones closer to  $k = 0$ ) correspond to the modulation of the input beam and are present for both low and high intensity. In the latter case, additional peaks appear at the higher harmonics due to MI. We also observed this harmonic generation in numerical simulations (bottom panels of Fig. 3), in good agreement with the experiments. In contrast, we did not observe such harmonics in the experimental results for  $k$  values within the stable regions ( $R < 1$  in Fig. 2), again in agreement with the theoretical prediction.

Figure 4 shows the instability windows for a structure with a different period (with 3.1 mm air between each pair of 1 mm glass slides). The instability bands shift towards lower  $k$ , as expected from the theoretical and numerical predictions. The peaks of the first two bands are at  $k = 5.3 \times 10^{-3}$  and  $k = 1.46 \times 10^{-2}$ , respectively, and a third band appears around  $k = 2.05 \times 10^{-2}$ . Once again, we obtain good agreement between experiment, numerics, and theory.

*Conclusions.* In the present work, we provided an experimental realization of modulational instability (MI) in a medium that is periodic in the evolution variable. We also described the location of the instability bands *quantitatively* using an analysis of the Hill equation obtained from a modulational stability analysis of plane-wave solutions of a nonlinear Schrödinger equation. For layered Kerr media with piecewise constant modulations of the nonlinearity, the Hill equation becomes the Kronig-Penney model, providing a direct association of the MI bands with the forbidden energy zones of that model. One of the unique features of the periodic medium in this respect is the opening of additional MI bands, such

as the 2nd and 3rd bands discussed in the present work. We compared our theoretical predictions for the modulationally unstable bands to those obtained experimentally and numerically (using Fourier-space diagnostics to elucidate the instability of the latter) and found very good agreement. We also observed higher spatial harmonics for modulationally unstable beams, revealing another characteristic trait of MI. The good agreement between theoretical, numerical, and experimental results suggests a variety of extensions in the present setting of layered Kerr media in the direction of analyzing the creation and dynamics of solitary waves that result from MI.

*Acknowledgements.* We acknowledge support from the DARPA Center for Optofluidic Integration (DP), the Caltech Information Science and Technology initiative (MC, MAP), and NSF-DMS and CAREER (PGK).

---

- [1] T. B. Benjamin and J. E. Feir, *J. Fluid. Mech.* **27**, 417 (1967).
- [2] L. A. Ostrovskii, *Sov. Phys. JETP* **24**, 797 (1969).
- [3] A. Hasegawa and Y. Kodama, *Solitons in Optical Communications* (Oxford University Press, Oxford, 1996).
- [4] T. Taniuti and H. Washimi, *Phys. Rev. Lett.* **21**, 209 (1968); A. Hasegawa, *Phys. Rev. Lett.* **24**, 1165 (1970).
- [5] See e.g. P. G. Kevrekidis and D. J. Frantzeskakis, *Mod. Phys. Lett. B* **18**, 173 (2004) for a review.
- [6] K. E. Strecker *et al.*, *Nature* **417**, 150 (2002).
- [7] L. Salasnich *et al.*, *Phys. Rev. Lett.* **91**, 80405 (2003); L. D. Carr and J. Brand, *Phys. Rev. A* **70**, 033607 (2004).
- [8] S. Wabnitz, *Phys. Rev. A* **38**, 2018 (1988).
- [9] M. Soljačić and J. D. Joannopoulos, *Nature Materials* **3**, 211 (2004).
- [10] J. Meier *et al.*, *Phys. Rev. Lett.* **92**, 163902 (2004).
- [11] A. Smerzi *et al.*, *Phys. Rev. Lett.*, **89**, 170402 (2002); F. S. Cataliotti *et al.*, *New J. Phys.* **5**, 71 (2003); B. Wu and Q. Niu, *Phys. Rev. A* **64**, 061603(R) (2001); V. V. Konotop, and M. Salerno, *Phys. Rev. A* **65**, 021602 (2002).
- [12] Y. S. Kivshar and M. Peyrard, *Phys. Rev. A* **46**, 3198 (1992).
- [13] B. A. Malomed, *Progress in Optics* **43**, 71 (2002); S. K. Turitsyn *et al.*, *C. R. Physique* **4**, 145 (2003).
- [14] I. Towers and B. A. Malomed, *J. Opt. Soc. Am. B* **19**, 537 (2002).
- [15] M. Centurion *et al.*, *Phys. Rev. Lett.*, **97**, 033903 (2006).
- [16] P. G. Kevrekidis *et al.*, *Phys. Rev. Lett.* **90**, 230401 (2003); see also F. Kh. Abdullaev *et al.*, *Phys. Rev. A* **67**, 013605 (2003); H. Saito and M. Ueda, *Phys. Rev. Lett.* **90**, 040403 (2003); G. D. Montesinos *et al.*, *Physica D* **191**, 193 (2003); B. A. Malomed, *Soliton Management in Periodic Systems* (Springer-Verlag, Berlin, 2006).
- [17] N. J. Smith and N. J. Doran, *Opt. Lett.* **21**, 570 (1996); F. Kh. Abdullaev *et al.*, *Phys. Lett. A* **220**, 213 (1996);
- [18] Z. Rapti *et al.*, *Phys. Scr.* **T113**, 74 (2004).
- [19] W. Magnus and S. Winkler, *Hill's Equation* (Wiley, New York, 1966).
- [20] C. Kittel, *Introduction to Solid State Physics* (John Wiley and Sons, New York, 1986).